

Numerical Simulation of the Thermal Comfort in a Model of a Passenger Car Cabin

Mikhail Konstantinov and Claus Wagner

Abstract Results of numerical simulations of the air flow including the heat transport, the thermal radiation and the thermal comfort of passengers in a model of passenger car cabin are presented. The computations have been performed by coupling flow simulations conducted with the Computational Fluid Dynamics (CFD) code OpenFOAM with simulations of the heat transport within the passengers using the finite-element code THESEUS-FE. The latter takes into account effects like blood flow, heat transfer through the skin and clothing as well as activity levels and ambient humidity in various layers with different heat transport characteristic. Based on these simulations four different ventilation variants known from the ventilation of aircraft cabins are analysed with respect to their performance regarding the thermal comfort of passengers and the their energy efficiency in future electric cars.

Keywords Passenger car · Thermal comfort model (TSM) · CFD · Cabin air flow

1 Introduction

In the past, the car manufacturers considerably improved the thermal comfort of the passengers by testing of different cabin ventilation techniques. Further improvements as well as the adaptation and optimization of these ventilation techniques for future electro cars will strongly rely in numerical flow simulations.

To predict the thermal comfort in numerical simulations numerous thermal sources have to be considered, one of which is the passenger itself. In principal, the human thermal comfort depends on the air temperature, the humidity, the mean radiant

M. Konstantinov (✉) · C. Wagner
Ilmenau University of Technology, Institute of Thermodynamics
and Fluid Mechanics, Am Helmholtzring 1, 98693 Ilmenau, Germany
e-mail: mikhail.konstantinov@dlr.de

C. Wagner
German Aerospace Center (DLR), Institute of Aerodynamics and Flow Technology,
Bunsenstr a e 10, 37073 G ottingen, Germany

temperature, the relative air velocity, the activity level and the insulation value of the clothing. Conventionally, in Computational Fluid Dynamics (CFD) methods, the permanent thermal boundary conditions are prescribed at the passenger-air interface [1]. There are more sophisticated numerical thermal comfort models, which consider the influence of the clothing and the human body by defining several layers with different heat conductivities and capacities and by computing the heat transport in the cardiovascular system [2–5]. Additionally, the influence of the human activity level and of the ambient humidity on the human's physiology is sometimes considered. Numerical predictions of comfort conditions in cabins usually rely on the coupling of CFD calculation with appropriate thermal comfort model. Such comfort calculations were conducted using commercial CFD codes (i.e. ANSYS CFX, StarCCM+) and comfort models [6–9] for different car cabins in the last 10 years.

Here, the objective is to adapt different ventilation techniques, known to be efficient for aircraft cabin, to a car cabin and to study and compare their performance with respect to the passengers' thermal comfort and their energy efficiency. The latter is of increasing importance, since the energy consumption of the air-conditioning system in electric cars determines their operating distance.

The thermal comfort simulations presented below rely on the developed at the DLR Göttingen [10] coupling of the finite volume method OpenFOAM, which solves the Reynolds-Averaged Navier-Stokes (RANS) equations using the Boussinesq approximation, with the commercial finite element program THESEUS-FE. Recently another concept of coupling between OpenFOAM and THESEUS-FE was performed on the cabin of VW e-Golf in [11].

2 Thermal Comfort Model

The here considered thermal comfort simulation are based on the solution of the mass, momentum and heat transport equations and the coupling to a heat transport simulation for a thermal manikin, the so-called FIALA-Manikin model [2, 3]. By using the THESEUS-FE software [12] the body of the considered thermal manikin consists of 54 body segments. To reduce their number and to save computational resources, the body segments were clustered to 14 segments. For example, the head, face and neck of the FIALA-Manikin were merged into one segment of our Thermal Comfort Model (TCM). Other merged segments are the torso, the left and right segments of the upper and lower arms, the hands, the upper and lower legs and the feet. Each of these body segments consists of several material layers. Additionally, individual clothing layers are defined for any of the above discussed segments. Finally, it must be noted that the core of each segment has its own attributes and that gender effects as well as differences in the human thermoregulation are not considered. For each body segment the following partial differential equation is solved in all layers to obtain the temperature changes in each material element:

$$\rho c \frac{\partial T}{\partial t} = k \left(\frac{\partial^2 T}{\partial r^2} + \frac{\omega}{r} \frac{\partial T}{\partial r} \right) + q_m + \rho_b c_b w_b (T_{b,a} - T) \quad (1)$$

Here ρ is the density, c the specific heat, k the thermal conductivity, T the temperature, q_m the metabolic heat flow density, w_b the blood perfusion rate and $T_{b,a}$ the calculated arterial temperature. The term $\rho_b c_b w_b (T_{b,a} - T)$ describes the contribution due to the arterial blood flow. The shape of the body elements is simplified by considering them as cylinders, except for the head which is modeled as a sphere. For all body elements, r denotes the radial coordinate. The dimensionless parameter ω is 1 for cylindrical body elements (for example the legs) and 2 for the spherical body element (head). Thus, Eq. (1) describes the law of energy conservation for each finite element in the material layers representing the skin, fat, muscles, bones, brain and so on.

The local clothing properties of each garment are prescribed according to the model of McCullough [13]. The clothing is defined through the thickness, clothing resistance, evaporation resistance, non-structural mass and specific heat. The thickness of 3 mm has been chosen for the torso and arms and legs, while the thickness of the feet amounted to 6 mm. We verified these clothing parameters in simulations of the thermal comfort of passengers in the cabin of the research aircraft Do728. The computed temperatures on the passengers were well supported by measurements conducted with an infrared camera [10].

The computed surface (T_{sf}) and skin (T_{sk}) temperatures allowed to estimate the following comfort parameters. First, an equivalent temperature T_{eq} is determined according to

$$T_{eq} = T_{sf} - \frac{R + C + E}{h_{cal}}, \quad (2)$$

where R , C and E symbolize the heat fluxes caused by radiation, convection and evaporation, respectively. Evaporation is estimated and calculated in THESEUS-FE based on a prescribed humidity. Further, h_{cal} denotes the combined heat transfer coefficient of the specific environment ($h_r + h_c$), where h_r stands for the radiation and h_c for the convection heat transfer coefficient. Finally, the equivalent temperature is the temperature of a homogeneous room with a radiation background temperature equal to the air temperature and low relative air speed.

There are two other important comfort parameters, namely the Zhang sensation and comfort indices. The Zhang local sensation index (ZSI) ranges from: 4 – “very hot”, 3 – “hot”, 2 – “warm”, 1 – “slightly warm”, 0 – “neutral”, –1 – “slightly cool”, –2 – “cool”, –3 – “cold”, –4 – “very cold”. This index indicates the temperature feeling.

In contrast, the Zhang local comfort index (ZLC) indicates the well-being and ranges from 4 (“very comfortable”), 2 (“comfortable”), 0 (“just comfortable”) to –2 (“uncomfortable”), –4 (“very uncomfortable”). For more details on the calculation of the comfort indices the reader is referred to [4, 5].

To exchange data between the RANS simulations and the thermal comfort computation, we developed an interface realizing the communication between the two codes. The detailed description of this interface can be found in [10, 14].

At the beginning of the simulations, the initial temperature on the surfaces of all body segments of the passengers is prescribed as follows: head – $T_{he} = 308$ K, torso – $T_t = 308$ K, upper arms – $T_{ua} = 306$ K, lower arms – $T_{la} = 306$ K, hands – $T_{ha} = 307$ K, upper legs – $T_{ul} = 305$ K, lower legs – $T_{ll} = 304$ K and feet – $T_{fo} = 304$ K. After 100 iterations the heat flux densities resulting from heat radiation and convection are computed and written to an output file. Reading this file, the thermal comfort simulation (THESEUS-FE) obtains the heat flux densities and calculates a new set of surface temperature boundary conditions by solving Eq. (1). The results can be interpreted as an estimated response of a typical human body to a specific thermal loading. Further, an “equivalent” temperature is computed which is used to assess the thermal comfort, as well as the surface (and skin) temperatures. The latter are then passed on to the RANS simulations by updating the surface temperature boundary condition through an intermediate output file. The whole procedure is repeated every 10 iterations of the RANS computations.

3 Computational Details of the Flow Simulations

The Reynolds-averaged Navier-Stokes (RANS) equations with the Boussinesq approximation are solved with second order linear upwind schemes for turbulence, scalar, vector and radiation fields provided in the source library of Engys edition of OpenFOAM.

Equations are discretized and integrated on a hybrid structured/unstructured mesh consisting of a total of 10 million cells which has been generated with the mesher of the commercial program StarCCM+. The thermal boundaries have been resolved with 5 wall layers and wall distances in wall units of the grid points next to the walls of $y^+ < 1$ in 92% of the wall cells. The size and the interior shape of the vehicle mock-up, i.e. the cabin, are deduced from the VW Polo. The corresponding CAD geometry and a cross-section of the mesh are presented in Fig. 1.

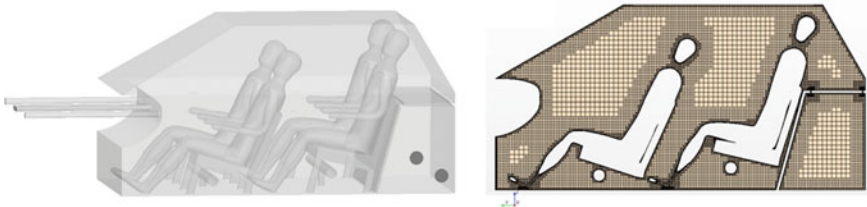



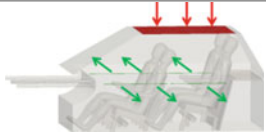
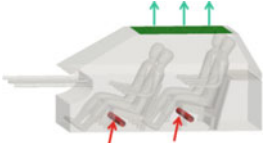
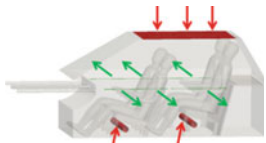
Fig. 1 CFD model of the generic car cabin (*left*) and a cut through the unstructured grid (*right*)

For each of the four passengers in the car cabin, 14 separate body segment boundary conditions are prescribed. The walls representing the sides, bottom, ceiling and windows are assumed to be adiabatic.

We examine the following four ventilation cases. The first one is denoted as the conventional reference case (REF) characterized by an air flow entering the cabin through four inlets from outside of the cabin and by outlets which are located in the luggage compartment. Individual ventilation settings are not regarded, all inlet jets have same intake angle 0° . In the second case fresh air enters the cabin through a trickle inlet ceiling (TI) and leaves it through two slots left and right of the cabin side. In the third variant the fresh air in the cabin is supplied through porous textile bags, the so-called cabin displacement ventilation (CDV) inlets and the trickle ceiling serves as an outlet. Finally, the last variant is a combination of the TI and CDV case—denoted as the hybrid (HYB) case. Here half of the air volume flux is contributed through textile bags close to the floor and the other half through the TI inlets at the ceiling while the air leaves the cabin through the side slots. More details of the considered cases are provided in the graphics shown in Table 1. It must be be noted that whether these four ventilation variants are suited for a real cars is not addressed in the present study, since the vehicle motion as well as solar radiation are not considered. Further, all walls except the surfaces of the passenger are assumed adiabatic. For all cases the overall inlet volume flux of $0.028 \text{ m}^3/\text{s}$ and an inlet temperature of 13.6 C° are the same. Thus, the performance of the ventilation cases can be compared in terms of the achieved passenger comfort and the mean cabin temperature.

The conducted turbulent flow simulations include the computation of heat radiation based on a Discrete Ordinates Model (DOM) with 40 rays. The simulations were carried out with the “buoyantBoussinesq” solver of OpenFOAM provided by the Engys GmbH, which integrates the RANS equations together with the $k-\omega/\text{SST}$ model [10]. As mentioned above, heat flux densities on the passenger’s surfaces are first computed and than passed on to the finite-element code THESEUS-FE which

Table 1 Sketches of the investigated ventilation cases

 <p>Reference (REF)</p>	 <p>Trickle inlets (TI)</p>
 <p>Cabin Displacement Ventilation (CDV)</p>	 <p>Hybrid (HYB)</p>

updates the surface body temperatures and determines several comfort parameters such as the perceived temperature. Then, the RANS simulations are continued for 10500 iterations.

4 Computed Flow Fields

Figures 2 and 3 reflect the streamlines and the surface temperatures of the passengers computed for the cases REF and HYB. For case REF, air enters the cabin through four round intakes leading to high velocity values in four distinct jets. The jets are reflected at the body of the passenger in the first row and rear seats which is the reason for the development of large scale circulations in front and behind the passengers. The temperature on the passengers' body is asymmetrical due to inhomogeneous velocity field (Compare the left and right upper arms by driver). For case REF, the temperature distribution is more homogeneous than for case HYB, although the surface temperatures of passengers are high. For this case the predicted velocity values are significantly higher than for the other ventilation cases. In contrast, case HYB is characterized by homogenous air distribution with low velocity values and overall lower temperatures and thus, better higher cooling efficiency. This can be explained with a larger inlet area and thus, lower inlet velocities. At the same time the vertical temperature distribution in the HYB variant is less homogeneous than in REF case.

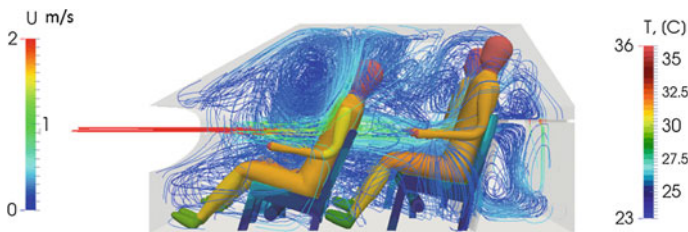


Fig. 2 Predicted streamlines and surface temperature distribution for the reference case

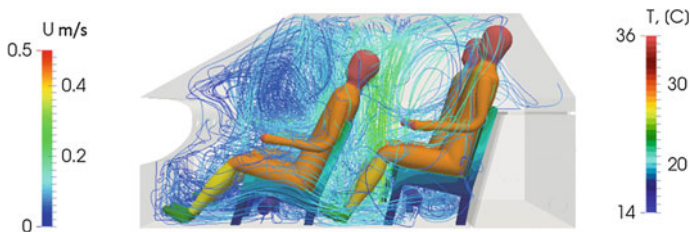


Fig. 3 Predicted streamlines and surface temperature distribution for the hybrid case

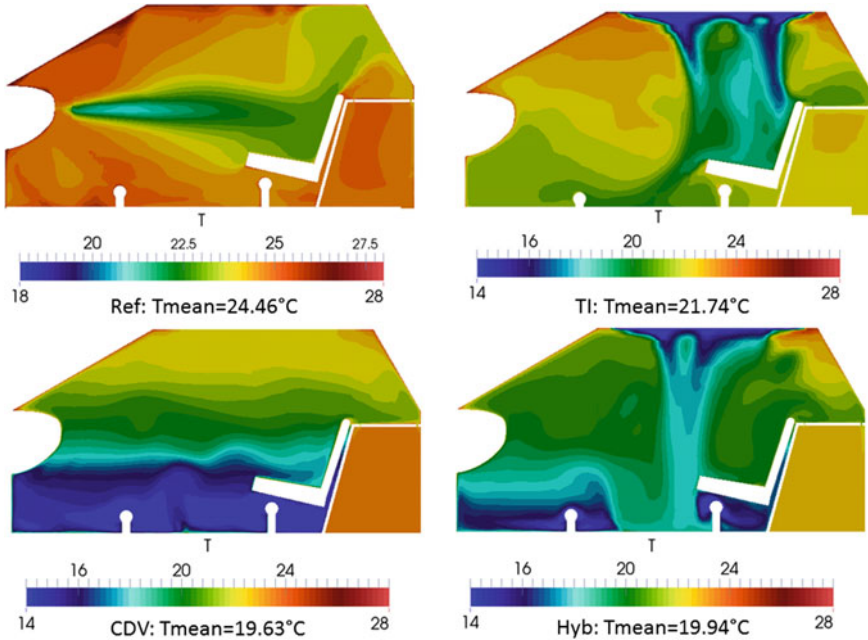


Fig. 4 Temperature distribution in middle cross-section for all considered variants

In Fig. 4 the predicted temperature distributions are presented in a middle cross-section of cabin. Higher temperature values are obtained for the cases Ref and TI in comparison to CDV and HYB. For CDV a significant vertical layer distribution of temperature is observed. Additionally, for the considered cases the following mean cabin temperatures are predicted: REF = 24.46 °C, TI = 21.74 °C, CDV = 19.63 °C, HYB = 19.94 °C.

With the above discussed temperature values it is possible to determine the heat removal efficiency (HRE) [15], defined in Eq. (3), which expresses the amount of energy needed to maintain a certain mean temperature in the cabin. The heat removal efficiency at a fixed volume flow rate is proportional to the amount of thermal energy, which the air has absorbed in the cabin, i.e. the temperature difference between the exhausted and the incoming air flow.

$$HRE = 0.5 \frac{(T_{exit} - T_{in})}{(T_{Cabin} - T_{in})} \tag{3}$$

The best possible HRE value for mixing ventilation is 0.5. The HRE can be greater as 0.5, if the heat source is located close to the exit. High HRE values indicate that less energy is needed to cool down the car cabin. Compared to the HRE value of 0.495 obtained for REF, all variants lead to higher HRE values, i.e. 0.52 for TI, 0.725 for CDV and 0.53 for HYB. This high HRE value obtained for the cabin displacement

ventilation (CDV) is in agreement with observations made for an aircraft cabin (see [15]). On the other hand, the cooling is inefficient if the difference between cabin temperature and incoming air temperature is high.

5 Comfort Predictions

The comfort predictions are evaluated based on the predicted Zhang indices and equivalent temperature for all cases. In Fig. 5 the distribution of Zhang sensation and local comfort index on the body of driver is presented. The overall Zhang comfort index ZC is “-0.39” for REF, “0.247” for TI, “0.5” for CDV and “0.6” for HYB. Although, all values are in the “just comfortable” range, case HYB reflects in the best comfort values. REF is less convenient, because in this case the sensation indices are significantly above the neutral value.

Finally, the predicted thermal comfort is analyzed based on the obtained local equivalent temperatures. The equivalent temperature reflects the comparable temperature of a homogeneous room assuming a radiation background temperature which is

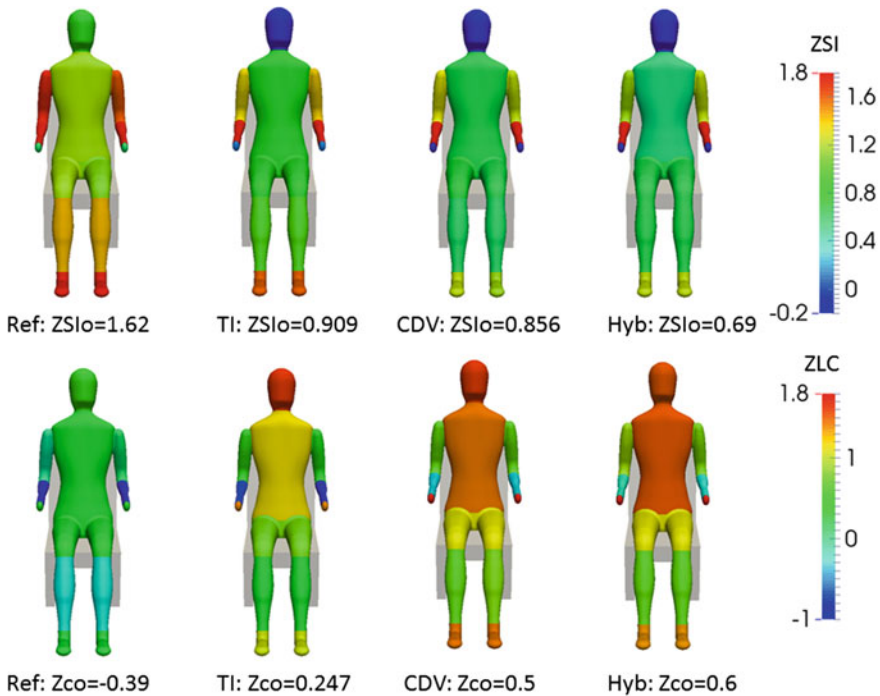


Fig. 5 Distribution of Zhang sensation (*above*) and local comfort (*below*) indices on passenger P1 for the four considered ventilation cases. Legend index “o” denotes overall

equal to the air temperature and low relative air speed. The comparison of distribution of equivalent temperatures for driver is presented in Fig. 6.

The ISO-14505-2 comfort zones, plotted as lines in Fig. 6, were defined analyzing a large number of experiments conducted for winter and summer conditions with samples of test persons and measurements of equivalent temperatures. Here, we consider the summer comfort zones and obtain that the predicted indices for CDV and HYB fall in the neutral zone while the values for REF and TI values are located in the warm, but comfortable, zone. CDV case reveals the higher temperature difference between head and feet, of about 7 °C. This large difference could be considered as uncomfortable. On the other hand, for REF of the obtained T_{eq} for the left and the right arms are different, which is also negative for the thermal comfort.

All important calculated parameters needed to evaluate ventilation concepts are summarized in Table 2. Here T_{cab} denotes the mean temperature in the cabin, ZSIo—Zhang Sensation Index of the whole body (temperature feeling) ZCo—Zhang Comfort Index of the whole body (well being). P1 indicates the driver and P4—the passenger in the second row left.

The comfort and efficiency values presented in Table 2 reveal that the mean cabin temperature obtained for CDV and HYB are nearly the same. Though, due to the specific temperature distribution in the cabin, the body elements by CDV case receive

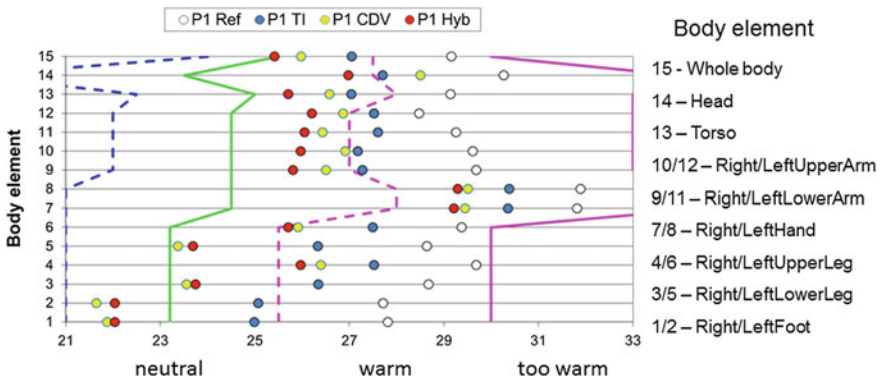


Fig. 6 Comparison of equivalent temperature on body elements of passenger P1

Table 2 Estimated comfort and energy efficiency for considered ventilation cases

Case	REF		TI		CDV		HYB	
T_{cab}	24.46 °C		21.74 °C		19.63 °C		19.94 °C	
HRE	0.495		0.52		0.725		0.53	
Seat	P1	P4	P1	P4	P1	P4	P1	P4
T_{eq}	29.16°	29.21°	27.05°	26.39°	25.98°	26.5°	25.42°	25.4°
ZSIo	1.626	1.647	0.909	0.797	0.856	1.02	0.691	0.71
ZCo	-0.39	-0.43	0.247	0.468	0.5	0.295	0.6	0.6

slightly higher temperature values than at HYB. This means that CDV case loads more heat flux in the cabin from occupants than HYB. Therefore, the CDV case has the higher HRE value followed by case HYB.

The equivalent temperatures for TI, CDV and HYB are located in neutral region. Highest well-being indices have been achieved in the case HYB.

6 Conclusions

The above discussed numerical thermal comfort predictions are based on solutions of the RANS equation together with the Boussinesq approximation, on the modeling of the thermal surface to surface radiation in a car cabin as well as on the coupling with the finite element code THESEUS. The developed coupling approach allows to predict the heat transport within the passengers, the perceived temperatures and the passenger comfort as well as the velocity and temperature distribution within the cabin. The work presented demonstrates clearly that the energy efficiency and the thermal comfort in the cabin depend on the used ventilation technique inlet design. By comparing the thermal comfort of the passengers and the heat removal efficiency obtained for different car cabin ventilation cases it was found that all alternative ventilation scenarios lead to better comfort indices than the conventional REF case with more homogeneous air flow within the cabin. The higher cooling efficiencies of CDV and HYB might recommend these ventilation techniques for future electric cars, with a preference for HYB which leads to the better comfort indices.

References

1. Konstantinov, M., Rütten, M., Lambert, M., Wagner, C.: Strahlung als wesentlicher Faktor der numerischen Simulation von Flugzeugkabineninnenströmungen für Komfortvorhersagen“, Deutsches Luft- und Raumfahrtkongress, Aachen, ID: 121285, (2009)
2. Fiala, D.: Dynamic simulation of human heat transfer and thermal comfort, Ph. D. Thesis. Inst. Energy Sustain. Dev., De Montfort University Leicester (1998)
3. Fiala, D., Lomas, K.J., Stohrer, M.: Computer prediction of human thermoregulatory responses to a wide range of environmental conditions. *Int. J. Biometeorol.* **45**, 143–159 (2001)
4. Zhang, H., Arens, E., Huizenga, C., Han, T.: Thermal sensation and comfort models for non-uniform and transient environments: part I: local sensation of individual body parts. *J. Build. Environ.* **45**, 380–388 (2010)
5. Zhang, H., Arens, E., Huizenga, C., Han, T.: Thermal sensation and comfort models for non-uniform and transient environments: part II: local comfort of individual body parts. *J. Build. Environ.* **45**, 389–398 (2010)
6. Han, T., Huang, L.: A Sensitivity Study of Occupant Thermal Comfort in a Cabin Using Virtual Thermal Comfort Engineering, SAE International, 2005–01-1509 (2005)
7. Chen, K., Kaushik, S., Han, T.: Thermal Comfort Prediction and Validation in a Realistic Vehicle Thermal Environment, SAE International, 2012–01-0645 (2012)

8. Lorenz, M., Fiala, D., Spinnler, M., Sattelmayer, T.: A Coupled Numerical Model to Predict Heat Transfer and Passenger thermal Comfort in Vehicle Cabins, SAE International, 2014–01-0664 (2014)
9. Zhang, Y., Meng, W., Chen, T., Hao, Y.: Cabin Thermal Comfort Simulation of Truck Based on CFD, SAE International, 2015–01-0344 (2015)
10. Konstantinov, M., Lautenschlager, W., Shishkin, A., Wagner, C.: Numerical simulation of the air flow and thermal comfort in aircraft cabins, In: Dillmann A. et al. (eds.) *New results in numerical and experimental fluid mechanics IX*, notes on numerical fluid mechanics and multidisciplinary design 124, Springer, 293–301 (2014)
11. Paulke, S., Köster, D., Hass, R., Bader, V., Menzel, S., Gubalke, A.: Thermische Simulationen einer Volkswagen e-Golf-Fahrzeugkabine unter Einbezug von thermischen Menschmodellen, SIMVEC, 17. Kongress, VDI-Berichten 2224, S. 555–588 (2014)
12. THESEUS-FE Theory Manual, Version 4.0. P+Z Engineering GmbH, Munich (2011)
13. McCullough, E.A., Jones, B.W., Huck, J.: A comprehensive data base for estimating clothing insulation. *ASHRAE Trans.* **91**, 316–328 (1985)
14. Konstantinov, M., Wagner, C.: Numerical simulation of the air flow and thermal comfort in a train cabin. In: *Proceedings of the second international conference on railway technology: research, development and maintenance*. Pombo, J., (Editor) Civil-Comp Press, Stirlingshire, United Kingdom, paper 328, 2014. doi:[10.4203/ccp.104328](https://doi.org/10.4203/ccp.104328)
15. Bosbach, J., Heider, A., Dehne, T., Markwart, M., Gores, I., Bendfeldt, P.: Evaluation of cabin displacement ventilation under flight conditions. In: *28th international congress of the aeronautical sciences ICAS2012*, 23. - 28. Sept. 2012, Brisbane, Australia. ISBN 978-0-9565333-1-9 (2012)